

# Characterizing Homogeneous Chemistry Using Well-Mixed Microeddies

Barry R. Lutz, Jian Chen, and Daniel T. Schwartz\*

Electrochemical Materials and Interfaces Laboratory, Department of Chemical Engineering, Box 351750, University of Washington, Seattle, Washington 98195-1750

Well-mixed reaction volumes are often sought in engineered microchemical devices and can be an important feature of naturally occurring physicochemical processes such as pitting corrosion. Steady streaming eddies can serve as well-mixed, easily controlled microliter chemical reactors for characterizing homogeneous chemical reactions. Here, steady streaming eddies are produced by oscillating a liquid-filled cuvette around a stationary cylindrical electrode (radius 406  $\mu\text{m}$ , length 1.6 cm) at audible frequencies (75 Hz). Oxidant (ferricyanide) electrochemically dosed at small rates ( $\leq 30$  nmol/s) from the cylindrical electrode accumulates to millimolar concentrations within the closed streamlines of each eddy, where it mixes and reacts with an antioxidant (vitamin C) present in the bulk solution. The composition in the eddy is controlled by varying the oxidant dosing rate and the bulk antioxidant concentration ( $\leq 10$  mM), as well as the cuvette oscillation amplitude. A simple algebraic mole balance is combined with Raman spectroscopy measurements of oxidant concentration in the eddy and bulk to determine the reaction rate law and homogeneous rate constant ( $45 \pm 9 \text{ M}^{-1} \text{ s}^{-1}$ ) for the antioxidant properties of vitamin C against ferricyanide. Numerical solutions to the full Navier–Stokes equations and species continuity equations illustrate the distribution of species during the reaction and general limitations to the assumption of a well-mixed eddy.

Homogeneous chemical reactions are often part of engineered microtechnologies,<sup>1,2</sup> but microchemical environments also arise naturally in many physicochemical processes such as pitting corrosion<sup>3–5</sup> and chemical etching.<sup>6–8</sup> With engineered microsystems, reaction boundary layers are commonly formed by bringing two reagent-containing streams together in a microchannel; lateral

interdiffusion forms a thin reaction zone whose width depends on the relative rates of diffusion and reaction. This configuration can perform useful local chemistry, like spatially directed materials synthesis,<sup>9</sup> and can serve as a platform for analytical determination of reaction rate parameters (through a comparison of spatially resolved spectroscopic data with multidimensional transport and reaction models).<sup>10–12</sup> On the other hand, if one seeks high conversion of chemical reagents into products, microscale convective mixing is normally attempted in order to provide more intimate contact and shorter diffusion paths between reagent streams.<sup>1,2,13</sup>

Naturally occurring physicochemical reaction phenomena are also sensitive to details of reagent mixing. For example, the microchemical environment in a corrosion pit is affected by the rate that oxidation products enter the pit from its corroding surface, homogeneous reactions involving those oxidation products, and the extent of reagent mixing inside the pit.<sup>3–5</sup> For all but the shallowest pits, the addition of bulk flow causes a recirculating eddy to form in the pit, resulting in reagent mixing that can accelerate or squelch further pit growth.<sup>4,5</sup> Unfortunately, because corrosion chemistry occurs inside a pit, acquiring in situ data can be difficult. More generally, any electrochemical process that obeys an electrochemical–chemical and electrochemical–chemical–electrochemical (EC and ECE, respectively) mechanism is sensitive to local mixing;<sup>14</sup> thus, controlled microelectrochemical environments can also be used to perform spatially directed materials synthesis.<sup>15</sup>

This work is largely motivated by a desire to develop quantitative tools for studying coupled EC and ECE processes in confined geometries, though the implications extend to engineered microchemical systems. Previously, we have shown that oscillating flows

\* To whom correspondence should be addressed. Phone: (206) 685-4815. Fax: (206) 543-3778. E-mail: dts@u.washington.edu.

- (1) Jensen, K. F. *Chem. Eng. Sci.* **2001**, *56*, 293–303.
- (2) Jakeway, S. C.; de Mello, A. J.; Russell, E. L. *Fresenius J. Anal. Chem.* **2000**, *366*, 525–539.
- (3) Lee, J. S.; Reed, M. L.; Kelly, R. G. *J. Electrochem. Soc.* **2004**, *151*, B423–B433.
- (4) Harb, J. N.; Alkire, R. C. *J. Electrochem. Soc.* **1991**, *138*, 3568–3575.
- (5) Harb, J. N.; Alkire, R. C. *J. Electrochem. Soc.* **1991**, *138*, 2594–2600.
- (6) Datta, M.; Landolt, D. *Electrochim. Acta* **2000**, *45*, 2535–2558.
- (7) Kondo, K.; Fukui, K.; Yokoyama, M.; Shinohara, K. *J. Electrochem. Soc.* **1997**, *144*, 466–470.
- (8) Georgiadou, M.; Alkire, R. J. *J. Electrochem. Soc.* **1993**, *140*, 1340–1347.

- (9) Kenis, P. J. A.; Ismagilov, R. F.; Takayama, S.; Whitesides, G. M.; Li, S. L.; White, H. S. *Acc. Chem. Res.* **2000**, *33*, 841–847.
- (10) Kamholz, A. E.; Weigl, B. H.; Finlayson, B. A.; Yager, P. *Anal. Chem.* **1999**, *71*, 5340–5347.
- (11) Pollack, L.; Tate, M. W.; Darnton, N. C.; Knight, J. B.; Gruner, S. M.; Eaton, W. A.; Austin, R. H. *Proc. Natl. Acad. Sci. U.S.A.* **1999**, *96*, 10115–10117.
- (12) Knight, J. B.; Vishwanath, A.; Brody, J. P.; Austin, R. H. *Phys. Rev. Lett.* **1998**, *80*, 3863–3866.
- (13) Nguyen, N. T.; Wu, Z. G. *J. Micromechan. Microeng.* **2005**, *15*, R1–R16.
- (14) Bard, A. J.; Faulkner, L. R. *Electrochemical Methods*; John Wiley & Sons: New York, 1980.
- (15) Li, S. L.; Macosko, C. W.; White, H. S. *Science* **1993**, *259*, 957–960.

in macroscopic vessels<sup>16</sup> and microchannel geometries<sup>17</sup> can be used to produce steady streaming microeddies with microliter and smaller volumes. When reagents are dosed into the microeddy, they are accumulated, creating a well-mixed core with constant concentration that is amenable to spectroscopic analysis.<sup>16,18</sup> Here we show that these well-mixed steady streaming microeddies can serve as predictable microchemical environments for characterizing homogeneous reactions. Steady streaming has found limited application for microscale mixing<sup>19–24</sup> and as a means for enhancing DNA hybridization rates to immobilized probes.<sup>25,26</sup> However, the desirable traits of a microeddy as a well-mixed reactor that can be tuned via the fluid oscillation properties have not been recognized. Moreover, having a well-mixed microeddy permits the use of simple algebraic continuously stirred tank reactor (CSTR) models to determine reaction rate laws and rate parameters. We demonstrate the approach by characterizing the homogeneous oxidation of vitamin C by an electrogenerated oxidant (ferricyanide).

## METHODS

The experimental system for steady streaming flow generation, flow visualization, electrochemical reagent dosing, and Raman concentration measurement has been described previously.<sup>16</sup> The flow was generated via sinusoidal oscillation (frequency  $\omega = 75$  Hz, displacement amplitude  $162 \leq s \leq 203 \mu\text{m}$ ) of a fluid-filled optical cuvette ( $1.5 \times 1.5 \times 2.5 \text{ cm}^3$ ) containing a stationary gold cylindrical electrode (radius  $a = 406 \mu\text{m}$ , length 1.6 cm). Thus, the flow oscillation amplitude was moderate for all experiments ( $0.4 \leq s/a \leq 0.5$ ).

Ferricyanide, the oxidant used here, was produced at the cylindrical electrode by galvanostatic oxidation of bulk ferrocyanide (50 mM) in the presence and absence of bulk vitamin C (ascorbic acid). Ferricyanide homogeneously oxidizes vitamin C via a two-step pH-dependent reaction<sup>27–29</sup> stabilized here by 1 M  $\text{Na}_2\text{SO}_4$  buffer (pH 2, deaerated). Solutions were freshly prepared to limit the influence of ferrocyanide decomposition at the low pH.<sup>30</sup> Electrochemical measurements verified that direct vitamin

C oxidation at the electrode was negligible. A two-compartment cuvette detailed elsewhere<sup>16</sup> allowed isolation of the flow compartment from the counter electrode. The bulk reservoir of vitamin C was sufficiently large to approximate steady-state conditions. The eddy reactor concentration at each condition was measured after 90 s of constant-current oxidant dosing.

Ferricyanide oxidant concentrations were quantified using Raman imaging spectroscopy<sup>16,31</sup> analyzed by principal component regression.<sup>32</sup> Two-dimensional Raman images of the OH-stretching region from water (not shown) were used to locate the cylinder and to position optical sampling volumes in the eddy core and in the bulk solution. Spectra from the CN-stretching region (near  $2100 \text{ cm}^{-1}$ ) were simultaneously acquired (514-nm excitation,  $\sim 50$ -mW power, 60–90-s exposure) from two optical sampling volumes probing  $\sim 0.5 \text{ nL}$  each. Ferricyanide oxidant was quantifiable to  $\sim 0.5 \text{ mM}$  using this scheme, whereas vitamin C was not detectable at the concentrations used here.

Experimental flow images were obtained by illuminating a flow cross section with a line-focused laser and collecting light scattered from entrained particles using a video microscope. The oscillation displacement amplitude ( $s$ ) was measured from time-exposed images of seeded silica particles ( $\sim 10 \mu\text{m}$ ) taken far from the cylinder under continuous illumination. Pulsed-laser illumination triggered by the sine wave voltage source allowed imaging of the steady component of flow. During flow imaging, long laser exposures ( $\sim 1 \text{ h}$ ) resulted in photodecomposition of the electrolyte, forming a deposit on the cylinder that could be released by electrooxidation to clearly mark the eddy boundary.

Density changes during chemical reaction can lead to buoyancy-induced natural convection. We have characterized buoyancy effects in this system through flow visualization and Raman concentration measurements of the eddy symmetry during oxidant dosing.<sup>33</sup> In our experiments, dosing rates and oscillation conditions are chosen so that buoyancy has a negligible effect on the driven eddy flow.

All experiments were performed at room temperature. The measured electrolyte kinematic viscosity was  $\nu = 0.013 \text{ cm}^2/\text{s}$ . Ferricyanide and vitamin C diffusion coefficients of  $3.95 \times 10^{-6}$  and  $4.27 \times 10^{-6} \text{ cm}^2/\text{s}$ , respectively, were determined from Levich plots of rotating disk limiting current data.

Two-dimensional flow and concentration fields were computed by finite element modeling using Femlab 2.3 (Comsol, Los Angeles, CA). The flow simulation geometry was bounded by a stationary central cylinder (radius  $a$ ) and an oscillating concentric outer cylinder (radius  $18a$ ) to approximate the experimental geometry. Analytical manipulation of the Navier–Stokes equations allowed sequential solution of the oscillating and steady flow components and improved simulation efficiency, as detailed elsewhere.<sup>18</sup> The analytical simplification is based on a small-amplitude oscillation assumption ( $s/a \ll 1$ ), though full solutions of the Navier–Stokes equations showed this approach captures many of the flow details up to moderate amplitudes. When buoyancy effects can be neglected, reagent and product distributions can be computed as passive scalar quantities (i.e., chemistry

(16) Lutz, B. R.; Chen, J.; Schwartz, D. T. *Proc. Natl. Acad. Sci. U.S.A.* **2003**, *100*, 4395–4398.

(17) Lutz, B. R.; Chen, J.; Schwartz, D. T. *Phys. Fluids* **2005**, *17*, 023601.

(18) Bowman, J. A.; Schwartz, D. T. *Int. J. Heat Mass Transfer* **1998**, *41*, 1065–1074.

(19) Suri, C.; Takenaka, K.; Yanagida, H.; Kojima, Y.; Koyama, K. *Ultrasonics* **2002**, *40*, 393–396.

(20) Rife, J. C.; Bell, M. I.; Horwitz, J. S.; Kabler, M. N.; Auyeung, R. C. Y.; Kim, W. J. *Sens. Actuators, A* **2000**, *86*, 135–140.

(21) Nishimura, T.; Murakami, S.; Kawamura, Y. *Chem. Eng. Sci.* **1993**, *48*, 1793–1800.

(22) Matta, L. M.; Zhu, C.; Jagoda, J. I.; Zinn, B. T. *J. Propul. Power* **1996**, *12*, 366–370.

(23) Carlsson, F.; Sen, M.; Lofdahl, L. *Eur. J. Mech. B* **2005**, *24*, 366–378.

(24) Liu, R. H.; Yang, J. N.; Pindera, M. Z.; Athavale, M.; Grodzinski, P. *Lab Chip* **2002**, *2*, 151–157.

(25) Boraker, D. K.; Bugbee, S. J.; Reed, B. A. *J. Immunol. Methods* **1992**, *155*, 91–94.

(26) Liu, R. H.; Lenigk, R.; Druyor-Sanchez, R. L.; Yang, J. N.; Grodzinski, P. *Anal. Chem.* **2003**, *75*, 1911–1917.

(27) Winograd, N.; Blount, H. N.; Kuwana, T. *J. Phys. Chem.* **1969**, *73*, 3456–3462.

(28) Bansch, B.; Martinez, P.; Zuluaga, J.; Uribe, D.; Vaneldik, R. Z. *Phys. Chem. – Int. J. Res. Phys. Chem. Chem. Phys.* **1991**, *170*, 59–71.

(29) Kagayama, N.; Sekiguchi, M.; Inada, Y.; Takagi, H. D.; Funahashi, S. *Inorg. Chem.* **1994**, *33*, 1881–1885.

(30) Leal, J. M.; Garcia, B.; Domingo, P. L. *Coord. Chem. Rev.* **1998**, *173*, 79–131.

(31) Schwartz, D. T.; Haight, S. M. *Colloids Surf., A* **2000**, *174*, 209–219.

(32) Haight, S. M.; Schwartz, D. T.; Lilga, M. A. *J. Electrochem. Soc.* **1999**, *146*, 1866–1872.

(33) Lutz, B. R. Ph.D. Thesis, University of Washington, Seattle, 2003.

does not affect flow). A subdomain of the computed steady flow field was used in the solution of the coupled species conservation equations to calculate the concentration fields of all reagents and products. Flow and concentration distributions computed for one quadrant occur symmetrically in the remaining three quadrants. All computations were performed using equations cast in an Eulerian frame of reference. Flow field simulations took  $\sim 2$  h on a 2.4-GHz computer, and reaction simulations using the flow field took  $\sim 45$  min. Analytical Stokes drift corrections<sup>34,35</sup> were used to transform velocity fields between Eulerian and Lagrangian frames of reference to allow comparison between specific experiments and the corresponding computations. Computed concentration fields are used to describe the general reactor behavior.

## RESULTS AND DISCUSSION

The interaction of a low-frequency fluid oscillation with a stationary cylinder produces a well-studied steady streaming flow, in which four symmetric eddies steadily circulate adjacent to the cylinder.<sup>18,34–37</sup> Figure 1 shows computed (upper) and experimental (lower) images for one quadrant of this steady streaming flow. The closed streamlines in the computed image clearly show one of the four eddies adjacent to the cylinder. The bold arc represents the dividing streamline that separates the eddy from the outer (“bulk”) fluid, which circulates throughout the container volume. The experimental image shows scattering from particles injected into the eddy from the cylinder surface, and the particle path lines clearly show the location of the dividing streamline (white arc). The dividing streamline and cylinder surface define a distinct volume of trapped recirculating fluid with microscopic dimensions. The eddy size and flow speed are governed by a dimensionless frequency,  $a^2\omega/\nu$ , and a dimensionless amplitude,  $s/a$ . Distinct eddies such as those shown in Figure 1 are created at moderate frequencies, roughly  $10 < a^2\omega/\nu < 1000$ . We have shown previously that these eddies accumulate and mix a chemical dosed from the surface, and the eddy composition is quantitatively controlled via the dosing rate and oscillation conditions.<sup>16</sup> Here, we consider steady-state homogeneous reaction between a reagent dosed from the cylinder and a reagent present in the bulk fluid.

When one or more chemical reagents are dosed into the eddy from the cylinder surface, and the bulk fluid possesses a homogeneous catalyst or additional reagent, each recirculating eddy serves as a well-mixed “vessel” for homogeneous reaction. Figure 2 illustrates the concept using computed cross sections of the recirculating flow (upper left) and various reactant and product species concentrations in the remaining three quadrants adjacent to the cylinder (hatched disk at center). The computed concentrations represent the steady-state reagent and product distributions when a substrate S, present in bulk solution, reacts with a reagent O, dosed from the cylinder, according to



The dosed species O could be delivered from a surface by

(34) Skavlem, S.; Tjøtta, S. *J. Acoust. Soc. Am.* **1955**, *27*, 26–33.

(35) Bertelsen, A.; Svardal, A.; Tjøtta, S. *J. Fluid Mech.* **1973**, *59*, 493–511.

(36) Holtmark, J.; Johnsen, I.; Sikkeland, T.; Skavlem, S. *J. Acoust. Soc. Am.* **1954**, *26*, 26–39.

(37) Raney, W. P.; Corelli, J. C.; Westervelt, P. J. *J. Acoust. Soc. Am.* **1954**, *26*, 1006–1014.

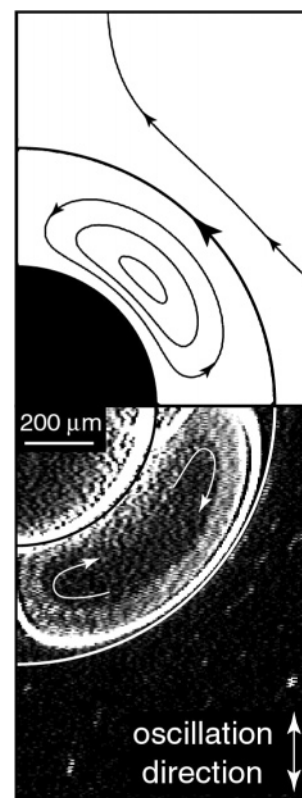


**Figure 1.** Computed (upper) and experimentally observed (lower) cross sections of steady streaming around a cylinder. Two of the four symmetric quadrants are shown, with the half cylinder cross section shown at left center. Closed streamlines in the computed image (streamline spacing  $\Delta\psi = 0.02$ ) indicate a recirculating eddy adjacent to the cylinder. The dividing streamline (bold arc) separates the eddy from the bulk solution. The experimental image ( $a = 406 \mu\text{m}$ ,  $\omega = 75$  Hz,  $s = 162 \mu\text{m}$ ) shows a particle stream ejected from the cylinder surface that circulates around the eddy perimeter and clearly identifies the dividing streamline (white arc inserted in the image for clarity). The computed flow field includes a Stokes drift correction to the Eulerian frame computations (see text).

enzymatic or catalytic surface reaction, electrochemical reaction, dissolution, or injection from a hollow fiber. In our experiments, the species O denotes the electrochemically generated oxidant ferricyanide, S is the antioxidant substrate vitamin C, and the homogeneous reaction products are R (ferrocyanide) and S\* (oxidized vitamin C). For the low pH used here, this multistep reaction is known to obey the overall rate law,<sup>27–29</sup>

$$r = k_h C_o C_s \quad (2)$$

where  $r$  is the homogeneous rate that O is reduced to R,  $k_h$  is the homogeneous rate constant, and  $C_o$  and  $C_s$  are the concentrations of O and S, respectively. The value of  $k_h$  reported in the literature is somewhat uncertain, with values cited in the range  $11 \leq k_h \leq 54 \text{ M}^{-1} \text{ s}^{-1}$  at  $25^\circ\text{C}$ <sup>27–29</sup> for electrolytes comparable to our experimental system. The computations in Figure 2 are for  $k_h = 30 \text{ M}^{-1} \text{ s}^{-1}$  and parameters that match the subsequent experimental data set.

Figure 2 (upper right and lower right) shows that the only spatial location where reagents O and S coexist with appreciable concentrations is within the well-mixed eddies. Thus, according

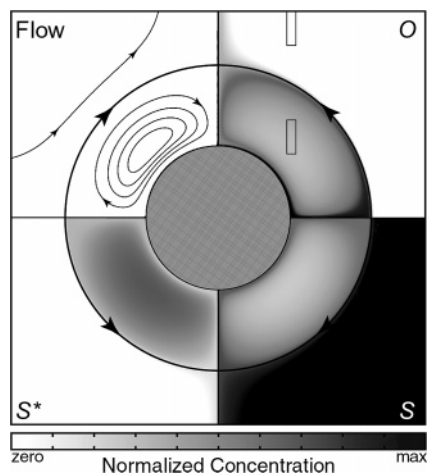


**Figure 2.** Computed cross sections of Eulerian frame streamlines and concentration distributions during steady-state homogeneous reaction around a cylindrical reagent dosing source. The cylindrical electrode cross section is shown by the crosshatched disk at the center. The flow field (upper left) is the Eulerian frame representation of the Lagrangian frame flow in Figure 1 (vertical fluid oscillations). Streamline spacing is  $\Delta\psi = 0.02$ . Labels in remaining quadrants refer to oxidant (O), antioxidant substrate (S), and deactivated antioxidant ( $S^*$ ) for the reaction of eq 1. Plotted concentrations are normalized by  $C_s^{\text{bulk}}$ ; the colorbar maximum (black) denotes  $C_o/C_s^{\text{bulk}} = 2$ , whereas  $\text{max} = 1$  for  $C_s/C_s^{\text{bulk}}$  and  $C_{s^*}/C_s^{\text{bulk}}$ . Dimensionless concentration fields are for a homogeneous rate constant  $k_h = 30 \text{ M}^{-1} \text{ s}^{-1}$  (average reported in refs 27–29), fluid properties  $\nu = 0.013 \text{ cm}^2/\text{s}$  and  $D = 4.1 \times 10^{-6} \text{ cm}^2/\text{s}$ , and representative experimental parameters ( $I/F = 6.2 \text{ nmol/s}$ ,  $C_s^{\text{bulk}} = 2 \text{ mM}$ ). The outlined boxes in the upper right quadrant represent the “point” Raman sampling locations used for experimental measurement of the oxidant (O) eddy core concentration,  $C_o^{\text{eddy}}$ , and oxidant bulk concentration,  $C_o^{\text{bulk}}$ .

to eq 2, homogeneous production of  $S^*$  and R should occur mainly within the eddies as well. Figure 2 (lower left) shows that product  $S^*$  indeed accumulates within the well-defined reaction zone created by the recirculating eddy. At steady state, homogeneous reaction within the eddy is balanced by diffusion of reagents and products across a thin mass-transfer boundary layer at the edge of the eddy. Fresh reagents entering at the eddy perimeter (O from the cylinder, S from the bulk solution) are mixed by convection and diffusion, and reaction products generated in the eddy enter the bulk solution by diffusion across the dividing streamline. Ideal mixing is characterized by perfectly uniform composition for all reagents and products within the reaction volume. While no real reactor can achieve this ideal limit, Figure 2 does show that reagents and products are well-distributed throughout the eddy core. This region of uniform concentration reduces the spatial accuracy needed for optical measurements and allows spatial averaging that greatly improves detection limits for the Raman measurements used here. The eddy and bulk concentrations are measured at “points” by averaging within the boxed regions in Figure 2.

A second advantage of a well-mixed reactor is the ability to describe the reaction volume using a simple algebraic reactor model. For this eddy, a lumped parameter material balance leads to a reactor model identical to that for a CSTR with separate feed streams for the two reagents. The rate that reagents and products are exchanged between the eddy and the bulk fluid can be

accurately determined using a time-averaged and spatially averaged mass-transfer coefficient,  $k_{\text{ds}}$  (cm/s), because convection dominates diffusion within the eddies (i.e., the eddy Peclet number is large,  $Pe = (s/a)^2\nu/D \gg 1$ , where  $D$  is the molecular diffusivity<sup>18</sup>). The molar rate that O is electrochemically dosed into the eddy is  $I/F$  for the one-electron charge transfer used here, where  $I$  is the dosing electrode current (C/s) and  $F$  is Faraday’s constant (96,486 C/mol). For the stoichiometry of eq 1, the steady-state algebraic mole balance equations for species O and S within the eddy reactor are,

$$rV = k_{\text{ds}}A_c(C_o^{\text{bulk}} - C_o^{\text{eddy}}) + I/F \quad (3)$$

$$1/2 rV = k_{\text{ds}}A_c(C_s^{\text{bulk}} - C_s^{\text{eddy}}) \quad (4)$$

respectively, where  $r$  is a homogeneous reaction rate (e.g., eq 2) using eddy concentrations,  $V$  is the volume of all four symmetric eddies,  $A_c$  is the dosing cylinder surface area, and concentration ( $C$ ) has a subscript that refers to the species and a superscript that refers to the location (either the eddy core or the bulk solution). The terms  $k_{\text{ds}}A_cC$  represent steady molar input or output rates across the dividing streamline. This simple reactor model will be used to determine the rate law and homogeneous rate constant for the homogeneous oxidation of vitamin C by ferricyanide.

The eddy reactor volume ( $V$ ) and mass-transfer coefficient ( $k_{\text{ds}}$ ) can be determined independently in the absence of homogeneous chemistry. The eddy volume of  $V = 30 \mu\text{L}$  is given by flow visualization with seed particles (Figure 1), including the small Stokes drift correction to the measured size. The mass-transfer coefficient is quantified by measuring  $(C_o^{\text{eddy}} - C_o^{\text{bulk}})$  as a function of the oxidant feed rate ( $I/F$ ), when there is no species S in the bulk solution (i.e.,  $C_s^{\text{bulk}} = 0$ ). In this no-reaction case (i.e.,  $r = 0$ ), eq 3 predicts a straight line with a slope of  $1/k_{\text{ds}}A_c$ . Figure 3A (filled circles) shows experimental measurements for this no-reaction case under the flow conditions of Figure 1. The data fit the predicted linear model (line through filled circles) and yield a slope of  $1/k_{\text{ds}}A_c = 500 \text{ s/cm}^3$ . The ratio  $V/k_{\text{ds}}A_c$  gives the mean reactor residence time,  $\tau_{\text{res}} = 15 \text{ s}$ , for fixed oscillation conditions of Figure 1. This means that, despite the small size of this reactor, the eddy circulates a dosed molecule for, on average, 15 s before it escapes to the bulk by diffusing across the dividing streamline.

When a known concentration of substrate is added to the bulk solution ( $C_s^{\text{bulk}}$ ), measurement of  $C_o^{\text{eddy}}$  as a function of oxidant feed rate ( $I/F$ ) and  $C_s^{\text{bulk}}$  creates a data set that can be used to quantify the reaction kinetics. Figure 3A (open symbols) shows the measured oxidant concentration in the eddy  $C_o^{\text{eddy}}$  as a function of oxidant feed rate ( $I/F$ ) at the flow conditions of Figure 1 and three values of  $C_s^{\text{bulk}}$  (in all cases  $C_o^{\text{bulk}} = 0$  within measurement error). For the fixed residence time, changes in  $C_s^{\text{bulk}}$  strongly influence the consumption of oxidant by homogeneous reaction. As  $C_s^{\text{bulk}}$  decreases, the homogeneous reaction slows, and the measured oxidant concentration approaches the data for no reaction (filled circles). Conversely, as  $C_s^{\text{bulk}}$  increases, the homogeneous reaction rapidly converts O dosed from the cylinder to R, resulting in a modest concentration of O in the eddy.

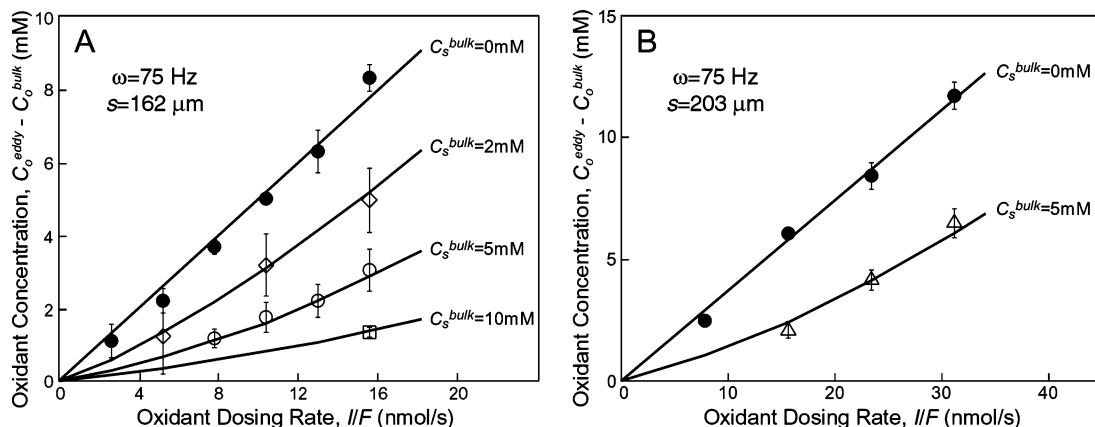


**Figure 3.** Measured oxidant concentration as a function of oxidant (ferricyanide) dosing rate and bulk substrate (vitamin C) concentration at an oscillation frequency  $\omega = 75$  Hz and oscillation amplitudes (A)  $s = 162 \mu\text{m}$  and (B)  $s = 203 \mu\text{m}$ . The filled circles denote the no-reaction case without vitamin C ( $C_s^{\text{bulk}} = 0$ ), and the best-fit lines give  $k_{\text{ds}}A_c$  for each oscillation condition as described in the text. Curves through the open symbols are from the reactor model (eq 5) using the best-fit rate constant ( $k_{\text{h}} = 45 \pm 9 \text{ M}^{-1} \text{ s}^{-1}$ ) determined by simultaneous regression of the three reaction data sets from (A). Error on  $k_{\text{h}}$  was calculated from  $\chi^2$  (90% confidence interval), and error bars on each data point represent one standard deviation resulting from multiple concentration measurements ( $n \geq 3$ ). The oxidant detection limit was  $\sim 0.5$  mM; concentrations of  $< 1$  mM were not included.

Equations 2–4 can be solved for the eddy oxidant concentration  $C_o^{\text{eddy}}$ ,

$$C_o^{\text{eddy}} = \frac{I}{2Fk_{\text{ds}}A_c} - \frac{k_{\text{ds}}A_c}{k_{\text{h}}V} - C_s^{\text{bulk}} + \sqrt{\left(\frac{I}{2Fk_{\text{ds}}A_c} - \frac{k_{\text{ds}}A_c}{k_{\text{h}}V} - C_s^{\text{bulk}}\right)^2 + 2\frac{I}{Fk_{\text{h}}V}} \quad (5)$$

where we have assumed that there is no bulk oxidant (i.e.,  $C_o^{\text{bulk}} = 0$ ) to match our experiments. In Figure 3A, the smooth curves passing through the open symbols result from the simultaneous nonlinear fit of eq 5 to all the reaction data. The best-fit model yields  $k_{\text{h}} = 45 \pm 9 \text{ M}^{-1} \text{ s}^{-1}$ , which falls in the range of the reported  $k_{\text{h}}$  values for the antioxidant properties of vitamin C (S) toward ferricyanide (O) at pH 2 and  $25^\circ\text{C}$ .<sup>27–29</sup> Figure 3A demonstrates variation of the reaction conditions for a fixed flow, and the simple reactor model describes the data well over the entire range.

The reaction conditions can be further varied via the flow conditions. The oscillation frequency and amplitude control the reactor volume<sup>18,34–37</sup> and the dividing streamline mass-transfer coefficient.<sup>18</sup> For example, Figure 3B shows results for a 25% increase in oscillation amplitude ( $s = 203 \mu\text{m}$ ) compared to Figure 3A for the same frequency, cylinder, and electrolyte. The Stokes-drift-corrected flow image (not shown) gave a slightly smaller eddy volume  $V = 24 \mu\text{L}$ . The slope of the line through the solid circles (no reaction),  $1/k_{\text{ds}}A_c = 370 \text{ s/cm}^3$ , indicates faster transport across the dividing streamline (i.e., larger  $k_{\text{ds}}$ ) when higher oscillation amplitude is used. The solid curve through the open symbols circles shows the model prediction from eq 5 with no adjusted parameters ( $k_{\text{h}}$  came from the independent data in Figure 3A). The mean residence time is reduced to  $\tau_{\text{res}} = 9$  s by a simple change in the flow conditions.

The variation of reactor conditions can be generalized by reformulating eq 5 as a dimensionless reactor design equation that relates the reagent conversion ( $X_o$ ) to the Damköhler number ( $Da$ ) and ratio of reagent feed rates ( $\phi$ ). Non-

dimensionalization of eq 5 provides

$$X_o = \frac{1}{2} + \frac{1}{2\phi} + \frac{1}{2Da\phi} - \sqrt{\left(\frac{1}{2} + \frac{1}{2\phi} + \frac{1}{2Da\phi}\right)^2 - \frac{1}{\phi}} \quad (6)$$

where the dimensionless variables are defined as  $X_o = 1 - Fk_{\text{ds}}A_cC_o^{\text{eddy}}/I$ ,  $\phi = I/2Fk_{\text{ds}}A_cC_s^{\text{bulk}}$ , and  $Da = Vk_{\text{h}}C_s^{\text{bulk}}/k_{\text{ds}}A_c$ . The reagent feed ratio ( $\phi$ ) is the molar dosing rate of O ( $I/F$ ) times the stoichiometric coefficient (from eq 1) divided by the rate that S enters the eddy across the dividing streamline ( $k_{\text{ds}}A_cC_s^{\text{bulk}}$ ).  $Da$  is the ratio of the mean reactor residence time ( $\tau_{\text{res}} = V/k_{\text{ds}}A_c$ ) to the characteristic reaction time ( $\tau_{\text{rxn}} = 1/k_{\text{h}}C_s^{\text{bulk}}$ ).<sup>38</sup> Just as in a conventional flow reactor, the two parameters that determine the residence time,  $V$  and  $k_{\text{ds}}A_c$ , were measured independent of homogeneous reaction. Equation 6 is identical to the reactor design equation for a macroscopic CSTR with separate inlet feed streams for O and S.

Figure 4 directly compares the data in Figure 3 with eq 6 by plotting the oxidant conversion,  $X_o$ , against the reagent feed rate ratio,  $\phi$ . The three reaction data sets from Figure 3A are shown by the open symbols, and the solid curves are the reactor model of eq 6 for the best-fit  $k_{\text{h}}$  found in Figure 3A. For a fixed residence time ( $\tau_{\text{res}} = 15$  s, solid curves),  $Da$  was varied by changing  $C_s^{\text{bulk}}$  as shown for the three data sets. At each fixed  $Da$ , variation of  $\phi$  leads to moderate changes in the oxidant conversion, while variation of  $Da$  allows access to a large range of reactor conversions. The dashed curve shows the reactor model for the smaller residence time ( $\tau_{\text{res}} = 9$  s) of Figure 3B (data points not shown for clarity). The two residence times lead to similar levels of oxidant conversion, but the reactor composition is quite different for the two cases.

One can also use measurements in a well-mixed micro-eddy to determine rate laws, if they are not already known. For

(38) Theones, D. *Chemical reactor development: from laboratory synthesis to industrial production*; Kluwer Academic Publishers: Dordrecht, 1994; pp 39–40, 200–201.

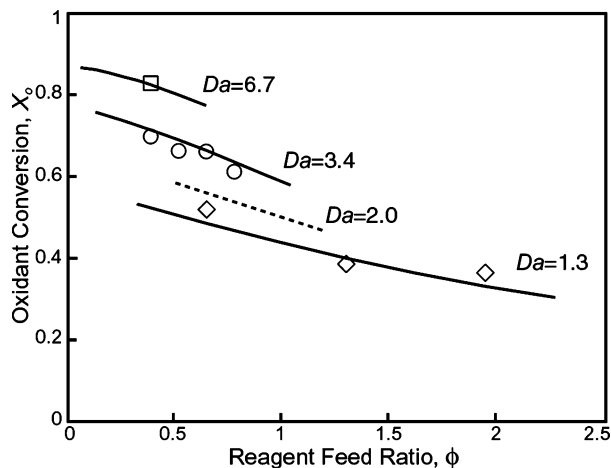


**Figure 4.** Dimensionless reactor plot for the data of Figure 3. Curves represent the ideal reactor model calculated from eq 6 using the best-fit  $k_h$  from Figure 3A. Data points and solid curves are for  $\tau_{res} = 15$  s (Figure 3A), and the dashed curve is for  $\tau_{res} = 9$  s (Figure 3B). For a fixed flow condition, each data set represents variation of the reagent feed rate ratio,  $\phi$ , at constant  $Da$  determined by  $C_s^{bulk}$  ( $\diamond$ , 2 mM;  $\circ$ , 5 mM;  $\square$ , 10 mM).

example, the general form for eq 2 is

$$r = k_h (C_o)^\gamma (C_s)^\delta \quad (7)$$

where  $\gamma$  and  $\delta$  are the reaction orders for oxidant and substrate, respectively. The data in Figure 3 can be used to find  $\gamma$ ,  $\delta$ , and  $k_h$  by manipulating eqs 3 and 4. The homogeneous reaction rate,  $r$ , can be calculated directly using eq 3 and measured oxidant concentrations. Equations 3 and 4 can then be combined to calculate the substrate concentration,  $C_s$ . Figure 5 shows that manipulation of the data in Figure 3 can be used to determine a multivariate best fit to eq 7, resulting in  $\gamma = 0.9$ ,  $\delta = 1.0$ , and  $k_h = 48 \text{ M}^{-0.9} \text{ s}^{-1}$ . The rate law determined from eq 7 is consistent with the known rate law for this two-step reaction ( $\gamma = 1$ ,  $\delta = 1$ ) and matches quite well the value of  $k_h$  found using the literature rate law.

Equations 3–5, and their nondimensional form, eq 6, are rigorously limited to the case where most reaction occurs in the well-mixed eddy core and negligible amounts of reaction occur in the thin transport boundary layer surrounding the eddy core. Rigorously, this means conditions where the Damköhler number is small compared to unity and the Peclet number is large. The conditions presented in Figure 2 are comparable to those found in our experimental system (moderate Damköhler numbers and large Peclet numbers). Clearly, under these conditions, most of the reaction occurs in the eddy core. However, the boundary layer around the edge of the eddy represents a finite fraction of the eddy volume, even for the high  $Pe$  number used ( $507 \leq Pe \leq 793$ ). The reagent distribution is similar to segregation of premixed reagents in a conventional two-input reactor, and use of the perfectly mixed reactor model introduces a systematic bias that causes the apparent rate constant to be higher than the actual value.<sup>38</sup> This systematic bias has a complex dependence on the reaction chemistry and details of mixing, but it is a feature of all real reactors when the overall reaction order is different from 1.

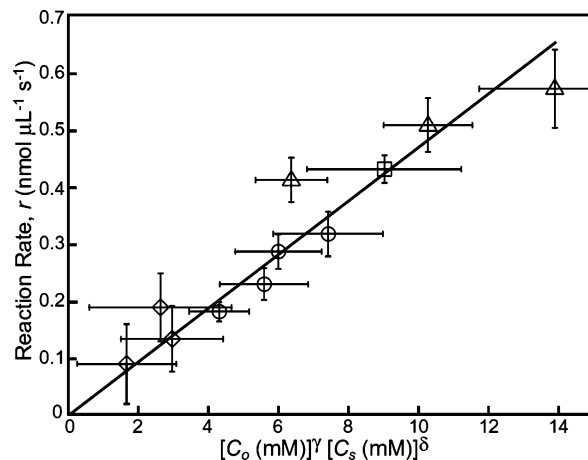


**Figure 5.** Reaction rate law plot for the data of Figure 3. Data include two residence times ( $\tau_{res} = 15$  s and  $\tau_{res} = 9$  s) and variation of both reagent feed rates (symbols are the same as in Figure 3). The volumetric reaction rate ( $r$ ) is calculated directly from the oxidant material balance (eq 3). The oxidant concentration is measured directly within the eddy ( $C_o = C_o^{eddy}$ ), and the substrate concentration ( $C_s = C_s^{eddy}$ ) is calculated from the material balance (eqs 3 and 4). The oxidant reaction order ( $\gamma$ ), the substrate reaction order ( $\delta$ ), and the homogeneous rate constant ( $k_h$ ) are determined by  $\chi^2$  minimization for simultaneous variation of the three parameters ( $\gamma = 0.9$ ,  $\delta = 1.0$ ,  $k_h = 48 \text{ M}^{-0.9} \text{ s}^{-1}$ ).

We are currently exploring how homogeneous kinetic measurements in this reactor are affected by  $Da$  and  $Pe$ . Nonetheless, the effects are expected to be small for these data, as our best-fit value for the rate constant in our example case falls well within the range reported in the literature.

## CONCLUSIONS

We have shown that the electrochemical dosing of a limiting reagent into a well-mixed microeddy containing a second reagent produces a predictable homogeneous reaction in the eddy. Electrochemically generated reagents are useful for many biological studies, where they can act as redox species for activation of NADPH, enzymes, and proteins.<sup>30,39,40</sup> Moreover, electrochemical generation is also the way oxidation products enter corrosion pits where they undergo further homogeneous chemistry. We are interested in applying the quantitative tools described here to tackle some of the more challenging microchemical problems that arise in coupled physicochemical systems such as pitting corrosion. However, reagents can be generated by other methods, such as dissolution from a solid, injection through a porous lumen, or generation from immobilized catalyst or enzyme. For example, Gleason and Carbeck used an average concentration boundary layer thickness to simplify analysis of immobilized enzyme products in a microchannel system.<sup>41</sup> Without much more complicated analysis, a steady streaming microeddy could be used to create a well-mixed and well-defined reaction volume for quantitatively interpreting the output from an immobilized enzyme or catalyst, including homogeneous following reactions or feedback inhibition mechanisms. More generally, the ability to create

(39) Ikeda, T.; Kano, K. *J. Biosci. Bioeng.* **2001**, *92*, 9–18.

(40) Kano, K.; Ikeda, T. *Anal. Sci.* **2000**, *16*, 1013–1021.

(41) Gleason, N. J.; Carbeck, J. D. *Langmuir* **2004**, *20*, 6374–6381.

strong flow adjacent to a solid boundary makes this type of flow ideally suited for mixing near reactive surfaces, where the effectiveness of typical mixing strategies is weakest. The fact that steady streaming microeddies can be created by any geometry that causes fluid streamlines bend (bumps, cavities, corners, etc.), and that they are easily generated and controlled in microfabricated systems,<sup>17</sup> suggests that there may be many other ways to use this interesting property of oscillating laminar flows.

#### **ACKNOWLEDGMENT**

We thank the National Science Foundation for major support provided by CMS-9872385 and the Center for Process Analytical Chemistry, an Industry/University Cooperative Research Center at the University of Washington, for partial support of this work.

Received for review September 15, 2005. Accepted December 27, 2005.

AC051646I